

Dark-Portal Leptogenesis in a Non-Holomorphic Modular Scoto-Seesaw Model

Salah Nasri^a , Labh Singh^b , Tapender^b , Surender Verma^b

^a*Department of physics, United Arab Emirates University, Al-Ain, UAE*

^b*Department of Physics and Astronomical Science, Central University of Himachal Pradesh, Dharamshala, Himachal Pradesh 176215, India*

E-mail: snasri@uaeu.ac.ae, sainilabh5@gmail.com,
tapenderphy@gmail.com, s_7verma@hpcu.ac.in

ABSTRACT: This work explores the neutrino phenomenology of the scotoseesaw model under non-holomorphic A_4 modular flavor symmetry providing a non-SUSY framework for realization of the modular symmetry. To prevent mixing between the beyond standard model fields associated with the tree and loop-level neutrino mass contributions, we assign even and odd modular weights to these sectors, respectively. The physical allowed ranges of oscillation parameters are used to identify the viable region of modulus parameter τ in its fundamental domain. With the complex modulus τ serving as the unique source of CP violation (all other parameters are real) the framework realizes successful low-scale leptogenesis through CP-violating decays of the lightest right-handed neutrino into Standard Model leptons and the Higgs boson. The requisite CP asymmetry arises from one-loop diagrams involving dark-sector states, obviating the need for degenerate mass spectra and thereby circumventing the usual resonant leptogenesis mechanism. The observation of a long-lived charged particle (η^\pm) in collider experiments would offer compelling evidence for the inert scalar sector of the model and provide a crucial experimental hint on the dark-sector assisted generation of neutrino masses and leptogenesis.

KEYWORDS: Modular symmetry; Radiative neutrino mass; Phenomenology; Leptogenesis; Dark matter.

Contents

1	Introduction	1
2	Model and Formalism	3
3	Neutrino Masses and Mixing	6
4	Lepton Flavor Violation	11
5	Leptogenesis	12
6	Conclusion	17
A	Non-Holomorphic Modular Flavor Symmetry	18

1 Introduction

The confirmed observation of neutrino oscillations provides definitive evidence that neutrinos are massive and undergo flavor mixing phenomena that necessitate physics beyond the Standard Model (SM) [1–6]. A fundamental theoretical challenge is the absence of right-handed neutrino counterparts in the SM, which precludes the generation of neutrino mass *via* the conventional Higgs mechanism. While the dimension-five Weinberg operator [7] offers a viable framework for neutrino mass generation, its ultraviolet completion and the specific flavor structure of neutrino sector remain open questions. Consequently, exploring beyond the standard model (BSM) scenarios is crucial for understanding the origin of neutrino mass. A wide spectrum of models has been proposed to align with oscillation data, including various implementations of the seesaw mechanism, radiative mass generation, and models involving extra dimensions [8–39]. A common feature in many of these frameworks is the introduction of sterile neutrinos: SM gauge singlets that act as right-handed partners. These sterile neutrinos couple to the active left-handed neutrinos *via* Yukawa interactions. The masses and coupling strengths of these sterile states can span many orders of magnitude, leading to diverse phenomenological implications. For instance, within the canonical type-I seesaw, the observed sub-eV neutrino masses naturally point to a very high mass scale for the right-handed neutrinos, around 10^{15} GeV, which is inaccessible to current experiments. However, alternative realizations of the seesaw mechanism—such as the inverse, linear, or extended seesaw, often constructed with discrete or continuous symmetries [40–46] can feature sterile neutrino masses at the TeV scale, rendering them potentially testable at current or future colliders. To date, neutrino oscillation experiments have precisely measured two mass-squared differences associated with atmospheric and solar neutrino oscillations. The existence of these two distinct mass scales may itself be a

clue, potentially indicating that the masses for the second and third generations originate from different underlying mechanisms.

To validate our assertion, we employ a recently proposed idea of the non-holomorphic modular symmetry, a non-SUSY realization of the holomorphic modular symmetry [47]. This approach is rooted in the construction of non-holomorphic modular forms, specifically polyharmonic Maaß forms. Unlike their holomorphic counterparts these forms are invariant under the modular group but are not required to be holomorphic, instead, they satisfy eigenfunction conditions under a Laplace-type differential operator. This expanded functional space incorporates both holomorphic and non-holomorphic components and accommodates modular forms of both positive and negative weights. Consequently, it enables the construction of more flexible and phenomenologically viable Yukawa coupling structures. Crucially, the rigid constraint of modular invariance is preserved, ensuring the model's predictive power while circumventing the limitations intrinsic to a purely holomorphic framework. Several works pertaining to the neutrino mass model building have already been done in the non-holomorphic modular symmetry [21, 48–66].

Further, the observed cosmic matter-antimatter asymmetry remains unexplained in the SM. Leptogenesis is a leading theoretical solution, proposing that this imbalance originated in the lepton sector [67–71]. It typically involves the out-of-equilibrium, CP-violating decay of heavy right-handed neutrinos in the early universe. This lepton asymmetry is subsequently converted into the observed baryon asymmetry *via* sphaleron processes. A notable feature of leptogenesis is its connection to the low-energy neutrino phenomenology through heavy right-handed degrees of freedom in the seesaw framework. The modular symmetry framework offers a highly predictive setting for leptogenesis, as the Yukawa couplings become functions of the complex modulus τ , which in turn acts as a natural source of CP asymmetry. Leptogenesis within modular-invariant theories has been extensively studied in holomorphic formulations [20, 22, 30–39] and some non-holomorphic extensions [21, 65, 66].

Motivated by this, we explored the *scoto-seesaw* framework [72, 73] where one mass square difference originates at the seesaw level and another at the one-loop (scotogenic) level. To forbid mixing between the tree-level and loop-level BSM sectors, distinct modular weights (κ) are assigned: tree-level fields carry even κ , whereas loop-level fields are odd under κ . In this setup, the heavy right-handed neutrino N_1 , responsible for the tree-level seesaw contribution, decays into the SM leptons and Higgs doublets. The dark sector, consisting of a chiral singlet fermion f , an inert scalar doublet, and a real scalar singlet s —all odd under κ —plays a multifaceted role: (i) it induces the one-loop radiative neutrino mass contribution, (ii) it mediates loop-level corrections to the N_1 decay amplitude whose interference with the tree-level process generates a non-zero CP asymmetry, and (iii) it offers a viable dark matter candidate within the model. The interaction $\mu_1 s \eta^\dagger H$, together with the Yukawa structure involving the fermion multiplet f and the singlet s , directly enters the one-loop diagrams responsible for leptogenesis. Consequently, the presence of s and the other BSM fields is not incidental but essential, as they generate the loop-induced CP

Fields	$SU(2)_L$	A_4	κ
L	2	3	2
e_R, μ_R, τ_R	1	1, 1', 1''	-2
H	2	1	0
N_1	1	1	2
N_2	1	1'	2
f	1	1	1
η	2	1	1
s	0	1	-1

Table 1: The particle content and charge assignments of the Scoto-Seesaw model under $SU(2)_L$ and A_4 non-holomorphic modular symmetry.

asymmetry, modify the washout structure, and allow successful leptogenesis at a comparatively lower scale without requiring near-degenerate heavy neutrinos.

The paper is organized as follows. In Section 2, we present the details of the model framework. Section 3 is devoted to explain the procedure involved in numerical estimation of neutrino masses and mixing parameters. In Section 4 we discuss the charged lepton flavor violation in the model. A discussion of dark-sector assisted leptogenesis, together with brief comments on the dark matter implications, is presented Section 5. Finally, conclusions are summarized in Section 6.

2 Model and Formalism

The modular symmetry-based Scoto-Seesaw model is given in the Table 1. The basic algebra of the modular symmetry has been given in Appendix A. To ensure that there is no mixing between the tree and loop level BSM fields, we have assigned even and odd weights to the tree and loop level fields.

The relevant scalar potential of the model is given by

$$V_{\text{tree}} = \mu_H^2 |H|^2 + \mu_\eta^2 |\eta|^2 + \lambda_1 |H|^4 + \lambda_2 |\eta|^4 + \lambda_3 |H|^2 |\eta|^2 + \lambda_4 |\eta^\dagger H|^2 + \tilde{\lambda}_5 [(\eta^\dagger H)^2 + \text{h.c.}] + \frac{\mu_s^2}{2} s^2 + \lambda_7 s^4 + \lambda_8 s^2 |H|^2 + \lambda_9 s^2 |\eta|^2 + (\mu_1 s H^\dagger \eta + \mu_1^* s \eta^\dagger H). \quad (2.1)$$

Here H is the SM Higgs doublet¹ and $\tilde{\lambda}_5 = \lambda Y_1^{(2)}$. Also, the scalar dark sector comprises of Higgs-type scalar doublet

$$\eta = \begin{pmatrix} \eta^+ \\ \frac{(\eta_R + i\eta_I)}{\sqrt{2}} \end{pmatrix}, \quad (2.2)$$

¹Although μ_1 , in general, can be complex, we take it as real in our study. It is to be noted that most of the terms in the scalar potential remain invariant under modular symmetry as given in [49].

and a real singlet scalar s . After spontaneous symmetry breaking, the charged and odd component of the η acquire mass as

$$m_{\eta^+}^2 = \mu_\eta^2 + \frac{1}{2}\lambda_3 v^2, \quad (2.3)$$

$$m_{\eta_I}^2 = \mu_\eta^2 + \frac{1}{2}(\lambda_3 + \lambda_4 - \tilde{\lambda}_5)v^2, \quad (2.4)$$

where v is the vacuum expectation value (vev) of the SM Higgs. In the (η_R, s) basis, the squared mass matrix is non-diagonal and is given by

$$M^2 = \begin{pmatrix} \frac{\partial^2 V}{\partial \eta_R^2} & \frac{\partial^2 V}{\partial \eta_R \partial s} \\ \frac{\partial^2 V}{\partial s \partial \eta_R} & \frac{\partial^2 V}{\partial s^2} \end{pmatrix} = \begin{pmatrix} \mu_\eta^2 + \frac{1}{2}(\lambda_3 + \lambda_4 - \tilde{\lambda}_5)v^2 & \mu_1 v \\ \mu_1 v & \mu_s^2 + \frac{1}{2}\lambda_8 v^2 \end{pmatrix}, \quad (2.5)$$

which can be diagonalized as

$$\begin{pmatrix} \eta_1 \\ \eta_2 \end{pmatrix} = \begin{pmatrix} \cos \theta & \sin \theta \\ -\sin \theta & \cos \theta \end{pmatrix} \begin{pmatrix} \eta_R \\ s \end{pmatrix}, \quad (2.6)$$

such that

$$\tan 2\theta = \frac{2\mu_1 v}{\mu_\eta^2 - \mu_s^2 + \frac{1}{2}(\lambda_3 + \lambda_4 - \tilde{\lambda}_5 - \lambda_8)v^2}. \quad (2.7)$$

The mass of CP even scalars is given by

$$\begin{aligned} m_{\eta_1}^2 &= \frac{1}{2} \left[\mu_\eta^2 + \mu_s^2 + \frac{1}{2}(\lambda_3 + \lambda_4 - \tilde{\lambda}_5 + \lambda_8)v^2 + \sqrt{\left(\mu_\eta^2 - \mu_s^2 + \frac{1}{2}(\lambda_3 + \lambda_4 - \tilde{\lambda}_5 - \lambda_8)v^2 \right)^2 + 4\mu_1^2 v^2} \right], \\ m_{\eta_2}^2 &= \frac{1}{2} \left[\mu_\eta^2 + \mu_s^2 + \frac{1}{2}(\lambda_3 + \lambda_4 - \tilde{\lambda}_5 + \lambda_8)v^2 - \sqrt{\left(\mu_\eta^2 - \mu_s^2 + \frac{1}{2}(\lambda_3 + \lambda_4 - \tilde{\lambda}_5 - \lambda_8)v^2 \right)^2 + 4\mu_1^2 v^2} \right]. \end{aligned}$$

Using a binomial expansion², the mass-squared eigenvalues of the inert scalars can be approximated as

$$m_{\eta_{1,2}}^2 \simeq \frac{1}{4} \left[2(\mu_\eta^2 + \mu_s^2) + v^2(\lambda_3 + \lambda_4 - \tilde{\lambda}_5) \pm \sqrt{(v^2(\lambda_3 + \lambda_4 - \tilde{\lambda}_5) - 2\mu_s^2 + 2\mu_\eta^2)^2 + 16\mu_1^2 v^2} \right] \quad (2.8)$$

The dark matter candidate in the model can be either a CP even (η_1, η_2) or a CP odd (η_I) scalar, depending on the mass spectrum considered. The relevant Yukawa Lagrangian for the charged leptons, based on the field content given in the Table 1 is given by

$$\mathcal{L} \supset \alpha_1 Y_3^{(0)} (\bar{L} H e_R) + \alpha_2 Y_3^{(0)} (\bar{L} H \mu_R) + \alpha_3 Y_3^{(0)} (\bar{L} H \tau_R) \quad (2.9)$$

where $Y_3^{(0)} = (Y_1^0, Y_2^0, Y_3^0)$ is an A_4 triplet modular form with weight 0. From this Lagrangian, charged lepton mass matrix can be written as

²We considered λ_8 small to eradicate unwanted mixing between SM Higgs and singlet scalar s .

$$M_\ell = v \begin{pmatrix} \alpha_1 Y_1^0 & \alpha_2 Y_3^0 & \alpha_3 Y_2^0 \\ \alpha_1 Y_3^0 & \alpha_2 Y_2^0 & \alpha_3 Y_1^0 \\ \alpha_1 Y_2^0 & \alpha_2 Y_1^0 & \alpha_3 Y_3^0 \end{pmatrix} = v \alpha_1 \begin{pmatrix} Y_1^0 & r_{21} Y_3^0 & r_{31} Y_2^0 \\ Y_3^0 & r_{21} Y_2^0 & r_{31} Y_1^0 \\ Y_2^0 & r_{21} Y_1^0 & r_{31} Y_3^0 \end{pmatrix},$$

where $r_{21} = \alpha_2/\alpha_1$ and $r_{31} = \alpha_3/\alpha_1$. The invariant Yukawa Lagrangian for neutrinos, including the Dirac Yukawa interactions and Majorana mass terms for the right-handed neutrinos, is given by

$$\mathcal{L} \supset \gamma \left(Y_3^{(4)} \bar{L} \tilde{H} N_1 + Y_3^{(4)} \bar{L} \tilde{H} N_2 \right) + \kappa_1 Y_1^{(4)} N_1 N_1 + \kappa_2 Y_{1'}^{(4)} N_2 N_2, \quad (2.10)$$

the right-handed neutrino mass matrix is then given by

$$M_R = \begin{pmatrix} \kappa_1 Y_1^{(4)} & 0 \\ 0 & \kappa_2 Y_{1'}^{(4)} \end{pmatrix}, \quad (2.11)$$

and Dirac neutrino mass matrix is

$$M_D = \gamma v \begin{pmatrix} Y_1^4 & Y_3^4 \\ Y_3^4 & Y_2^4 \\ Y_2^4 & Y_1^4 \end{pmatrix}, \quad (2.12)$$

where $Y_3^{(4)} = (Y_1^4, Y_2^4, Y_3^4)$ is A_4 triplet modular form with weight 4. The neutrino masses generated by Type-I seesaw is given by

$$(m^\nu)_{\text{tree}} = -M_D M_R^{-1} M_D^T. \quad (2.13)$$

Additionally, the model exhibits a scotogenic nature. The relevant Yukawa Lagrangian, which is important for the one-loop generation of neutrino mass can be expressed as

$$L = \beta_L Y_3^{(4)} \bar{L} \tilde{\eta} f + \kappa_S Y_1^{(2)} f f + a Y_1^{(2)} \bar{N}^c f s. \quad (2.14)$$

The loop-induced neutrino mass matrix takes the form

$$(m_{ij}^\nu)_{\text{loop}} = F(m_{\eta_1}, m_{\eta_2}, m_{\eta_I}) M_f h_i h_j, \quad (2.15)$$

where $M_f = \kappa_S Y_1^{(2)}$, and $F(m_{\eta_1}, m_{\eta_2}, m_{\eta_I})$ denotes the loop function

$$F(m_{\eta_1}, m_{\eta_2}, m_{\eta_I}) = \frac{1}{32\pi^2} [\cos \theta F(m_{\eta_1}) + \sin \theta F(m_{\eta_2}) - F(m_{\eta_I})], \quad (2.16)$$

with

$$F(m_x) = \frac{m_x^2}{M_f^2 - m_{\eta_x}^2} \ln \frac{m_x^2}{M_f^2}. \quad (2.17)$$

The neutrino mass matrix generated at the loop level is

$$(m^\nu)_{\text{loop}} = \beta_L^2 M_f \begin{pmatrix} (Y_1^4)^2 & Y_1^4 Y_2^4 & Y_1^4 Y_3^4 \\ Y_1^4 Y_2^4 & (Y_2^4)^2 & Y_2^4 Y_3^4 \\ Y_1^4 Y_3^4 & Y_2^4 Y_3^4 & (Y_3^4)^2 \end{pmatrix} F(m_{\eta_1}, m_{\eta_2}, m_{\eta_I}). \quad (2.18)$$

Input Parameters	Range
$\text{Re}[\tau]$	$\pm[0.0, 0.5]$
$\text{Im}[\tau]$	$[0.8, 1.5]$
γ	$[10^{-6}, 1]$
β_L	$[10^{-6}, 1]$
$\kappa_{1,2}$ (GeV)	$[10^5, 10^{10}]$
κ_s (GeV)	$[10^5, 10^{10}]$
$v\alpha_1$ (GeV)	$[10^{-3}, 10^{-2}]$
r_{21}	$[10^2, 1.5 \times 10^3]$
r_{31}	$[10^2, 1.5 \times 10^3]$
m_{η_1} (GeV)	$[500, 10^3]$
$\Delta m^2 = m_{\eta_1}^2 - m_{\eta_1}^2$ (GeV)	$[10^{-3}, 10]$
μ_1 (GeV)	$[10, 10^4]$

Table 2: The ranges of the parameters used for the numerical scan.

Considering Eqns. (2.13) and (2.18), the total neutrino mass matrix is given by

$$M^\nu = (m^\nu)_{\text{tree}} + (m^\nu)_{\text{loop}}. \quad (2.19)$$

The next step is to ascertain the viability of the model to reproduce low energy neutrino phenomenology which will help to identify the allowed parameter space of, initially, free parameters. In order to get the predictions for the neutrino oscillation parameters, we will numerically diagonalize M^ν in the next section.

3 Neutrino Masses and Mixing

The neutrino mass matrix given by Eqn. (2.19) is diagonalized using the relation $U_\nu^T M^\nu U_\nu = \text{diag}(m_{\nu_1}, m_{\nu_2}, m_{\nu_3})$. The mixing matrix $U_{\text{PMNS}} = U_L^\dagger U_\nu$, since the charged lepton mass matrix is not diagonal in the flavor basis. Now, the mixing angle can be extracted from U_{PMNS} as

$$\sin^2 \theta_{13} = |U_{13}|^2, \quad \sin^2 \theta_{12} = \frac{|U_{12}|^2}{1 - |U_{13}|^2}, \quad \sin^2 \theta_{23} = \frac{|U_{23}|^2}{1 - |U_{13}|^2}, \quad (3.1)$$

where U_{mn} are elements of U_{PMNS} . Further, the CP invariants sensitive to Majorana phases can be written in terms of the elements of the PMNS matrix

$$I_1 = \text{Im} [U_{11}^* U_{12}], \quad (3.2)$$

Observable	best-fit $\pm 1\sigma$ (NH)	best-fit $\pm 1\sigma$ (IH)	3σ range (NH)	3σ range (IH)
θ_{12} [°]	$33.8^{+0.7}_{-0.6}$	$33.8^{+0.7}_{-0.6}$	$31.3 \rightarrow 36.3$	$31.3 \rightarrow 36.3$
θ_{23} [°]	$49.1^{+0.9}_{-1.0}$	$49.2^{+0.9}_{-1.0}$	$39.8 \rightarrow 51.9$	$40.2 \rightarrow 52.1$
θ_{13} [°]	$8.55^{+0.13}_{-0.14}$	$8.57^{+0.13}_{-0.14}$	$8.2 \rightarrow 8.9$	$8.2 \rightarrow 8.9$
Δm_{21}^2 [10 $^{-5}$ eV 2]	$7.42^{+0.21}_{-0.20}$	$7.42^{+0.21}_{-0.20}$	$6.82 \rightarrow 8.04$	$6.82 \rightarrow 8.04$
Δm_{31}^2 [10 $^{-3}$ eV 2]	$+2.510^{+0.027}_{-0.027}$	$-2.490^{+0.026}_{-0.028}$	$+2.43 \rightarrow +2.58$	$-2.56 \rightarrow -2.42$
m_e/m_μ	0.004737	0.004737	—	—
m_μ/m_τ	0.058823	0.058823	—	—

Table 3: The neutrino oscillation observables from NuFIT 6.0 [74]. The values of the mass ratios of charged leptons have been taken from Ref. [75].

$$I_2 = \text{Im} [U_{11}^* U_{13}] . \quad (3.3)$$

Using effective Majorana mass

$$m_{\beta\beta} = |U_{11}^2 m_1 + U_{12}^2 m_2 + U_{13}^2 m_3| , \quad (3.4)$$

the model prediction for $m_{\beta\beta}$ is, also, investigated. We numerically diagonalize the neutrino mass matrix in Eqn. (2.19) and elucidate predictions for the neutrino observables. In order to ascertain the allowed parameter space, we define the χ^2 function as

$$\chi^2 = \sum_{i=1}^7 \left(\frac{P_i - P_i^0}{\sigma_i} \right)^2 , \quad (3.5)$$

where P_i represents the observables predicted by the model, P_i^0 the central value and σ_i represents the error corresponding to 1σ level as shown in Table 3. We have sampled the seven observables in this study which include three mixing angles, two mass-squared differences (Δm_{21}^2 and Δm_{31}^2), and two lepton mass ratios (m_e/m_μ and m_μ/m_τ) (see Table 3). We explore the parameter space (given in Table 2) using 10^9 samples in Monte Carlo simulations with mass hierarchy constraint $M_{N_1} < M_f << M_{N_2}$. The experimental input values used in our analysis are summarized in Table 3. These parameters demonstrate how well the model reproduces the observed neutrino mixing angles in the case of normal hierarchy (NH) yielding a minimum chi-square value of $\chi_{\min}^2 = 0.28$. The model predictions are illustrated through correlation plots obtained for $\chi^2 \leq 25$ where the solid black star denotes the best-fit point corresponding to $\chi_{\min}^2 = 0.28$. Fig. 1a presents the allowed region of the complex modulus $\tau = \text{Re}[\tau] + i \text{Im}[\tau]$ that remains consistent with the neutrino oscillation data. We find that the data are well fitted with $\text{Re}[\tau] \sim \pm 0.26$ and $\text{Im}[\tau] \sim 0.97$. The corresponding Yukawa couplings are displayed in Fig. 2. The predicted neutrino mixing angles lie within their 3σ experimental ranges as shown in Fig. 1b and 1c. Fig. 1d illustrates the correlation between the atmospheric mixing angle θ_{23} and the Dirac-type CP -violating phase δ . We observe that the model exhibits non-zero CP violation with Dirac phase δ being highly constrained to lie in the first and fourth quadrants. While NO ν A data allow normal ordering with $\delta \in [0^\circ, 180^\circ]$ and inverted ordering

$\theta_{12}(\circ)$	$\theta_{13}(\circ)$	$\theta_{23}(\circ)$	$\delta(\circ)$	$\Delta m_{21}^2(\text{eV}^2)$	$\Delta m_{31}^2(\text{eV}^2)$	$\text{Re}[\tau]$	$\text{Im}[\tau]$
34.00	8.56	43.15	289.04	7.5×10^{-5}	2.5×10^{-3}	0.26	0.98

Table 4: The best-fit values for the neutrino oscillation parameters obtained for a minimum χ^2 value of 0.28 for NH.

Parameter	Value	Parameter	Value
κ_1 (GeV)	7.90×10^5	κ_2 (GeV)	6.69×10^8
γ	9.52×10^{-6}	κ_S (GeV)	5.22×10^8
β_L	1.00	m_{η_1} (GeV)	6.98×10^2
ΔM_η^2 (GeV)	9.87×10^{-3}	$v\alpha_1$ (GeV)	4.10×10^{-3}
r_{21}	1.32×10^3	r_{31}	1.67×10^2
M_{N_1} (GeV)	1.21×10^6	M_{N_2} (GeV)	7.24×10^8
M_f (GeV)	3.09×10^7	$\text{Br}(\mu \rightarrow e\gamma)$	5.43×10^{-28}

Table 5: The values of the model parameters obtained from the χ^2 analysis corresponding to the $\chi^2_{min} = 0.28$ for the NH.

with $\delta \in [180^\circ, 360^\circ]$ [76], the T2K experiment favors values around $\delta \simeq 270^\circ$ for both hierarchies [77]. This region partially overlaps with the NO ν A and T2K-preferred normal ordering solution. The future precision measurements will therefore provide a decisive test for this framework. The predictions for the effective Majorana mass $m_{\beta\beta}$ as a function of the lightest neutrino mass m_1 are shown in Fig. 1e. The allowed region corresponds to the parameter space consistent with neutrino oscillation data in the case of NH. The model predicts $m_{\beta\beta}$ values that lie below the current experimental limits from KamLAND-Zen [78] and within the future sensitivities of LEGEND-1000 [79] and nEXO [80]. The observation of neutrinoless double beta decay ($0\nu\beta\beta$) in the upcoming experiments with refined sensitivities will therefore provide a critical test of the framework. The correlation between the invariants I_1 and I_2 (Eqns. (3.2)–(3.3)) is shown in Fig. 1f. The results indicate small but non-zero values of $I_{1,2}$, implying non-zero Majorana-type CP violation. Furthermore, we have investigated the parameter space for the inverted neutrino mass hierarchy. The model excludes the IH scenario as illustrated in Fig. 3. The figure illustrates the correlation between the mixing angles θ_{12} and θ_{23} , showing that θ_{23} falls outside the 3σ range of the global data, thereby, confirming the incompatibility with IH scenario. While the preference for NH is consistent with global analyses, the prediction of a first-octant solution for θ_{23} is in mild tension with the slight upper-octant preference reported by T2K and NO ν A. This discrepancy highlights a key testable prediction of our model. The best-fit values of neutrino observables and corresponding model parameters are given in Table 4 and 5, respectively.

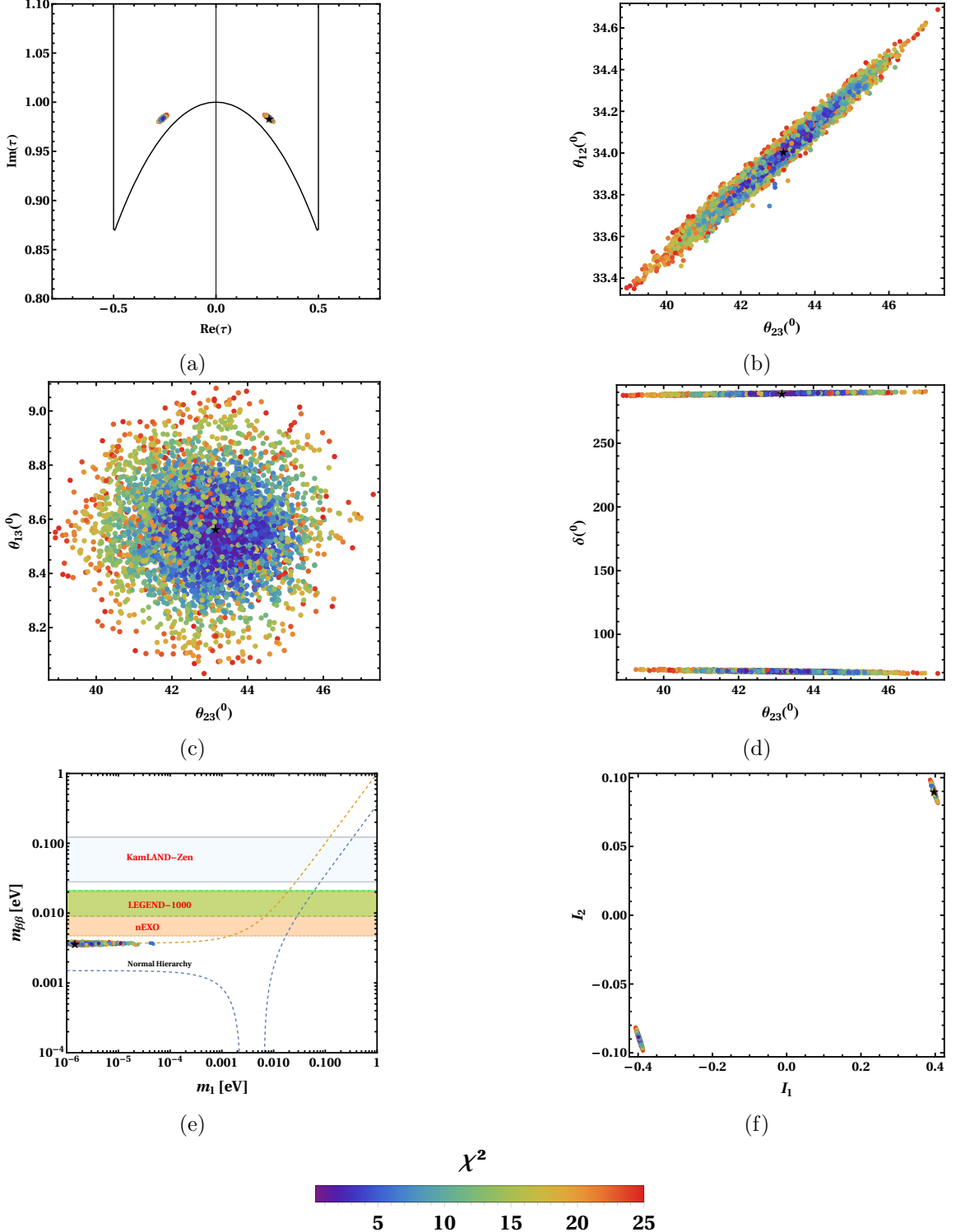


Figure 1: The allowed parameter space of the complex modulus τ and predicted ranges of neutrino observables such as mixing angles, Dirac type CP phase, effective Majorana mass, and Majorana CP invariants. The black star (\star) corresponds to the best-fit value obtained for $\chi^2_{min} = 0.28$.

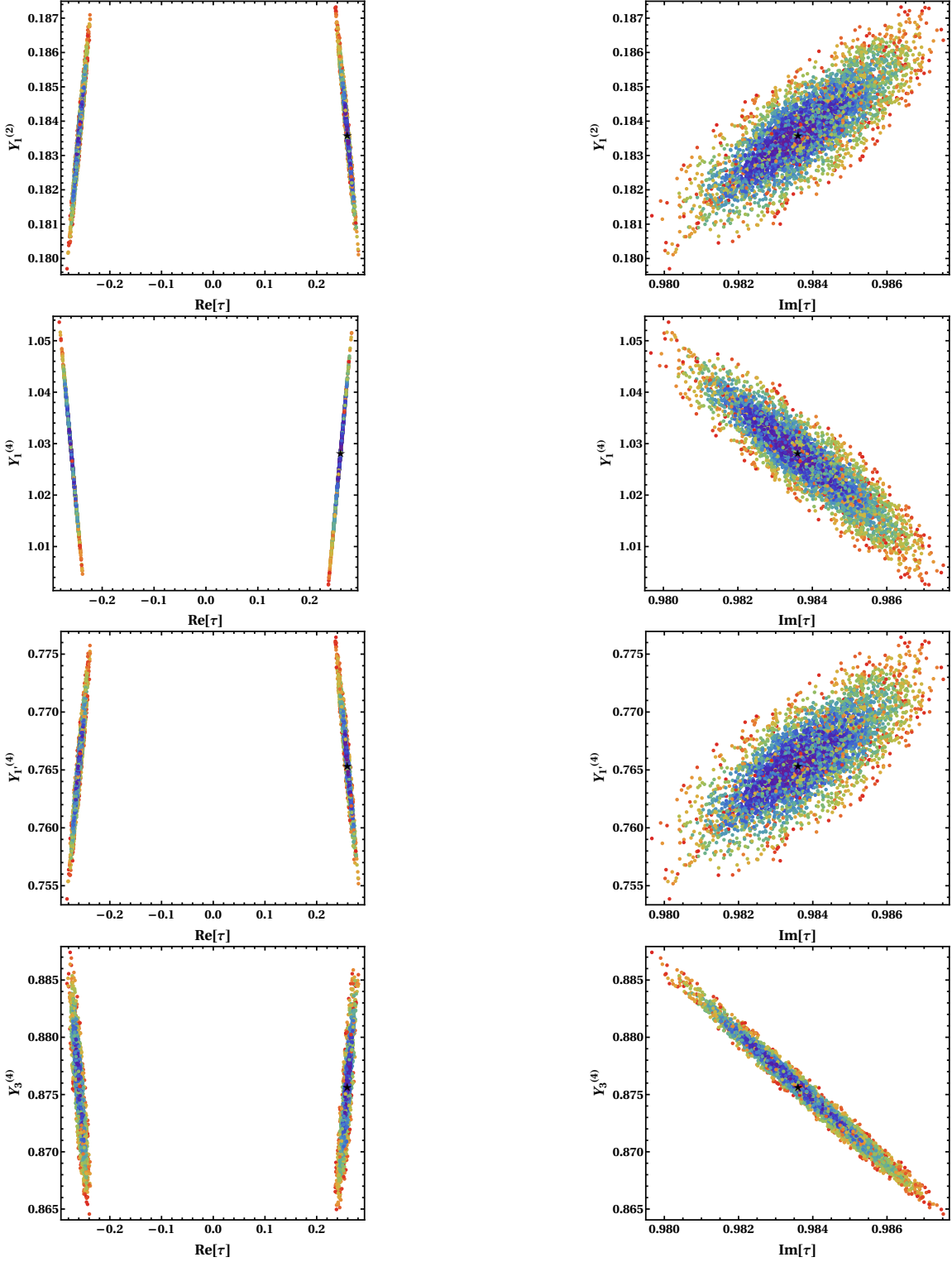


Figure 2: The variation of Yukawa couplings with real and imaginary part of complex modulus τ . The color code is same as for Fig. 1

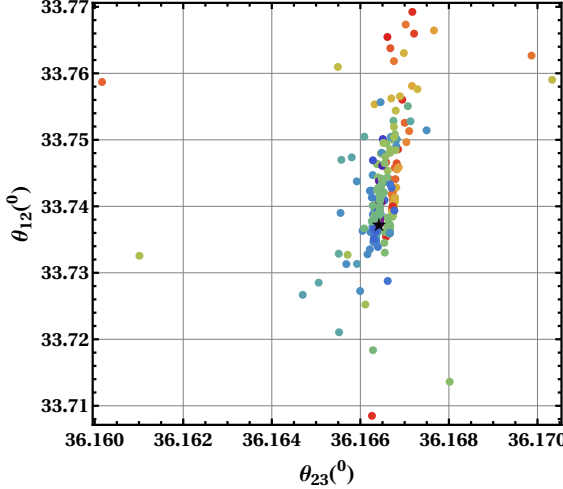


Figure 3: The correlation between atmospheric (θ_{23}) and solar (θ_{12}) mixing angle for IH.

4 Lepton Flavor Violation

One of the key low-energy signatures of physics beyond the SM is the presence of charged lepton flavor-violating (LFV) decays. In Scotogenic frameworks, the presence of new particles involved in the loop can induce sizable contributions to these processes. Among the various LFV channels, the decay $\mu \rightarrow e\gamma$ provides the strongest experimental constraint, with current upper limit $\text{Br}(\mu \rightarrow e\gamma) < 4.2 \times 10^{-13}$ [81]. In our analysis, we impose this bound to restrict the parameter space of the model. The branching ratio for the radiative decay $\mu \rightarrow e\gamma$ is [82]

$$\text{BR}(\mu \rightarrow e\gamma) = \frac{3(4\pi)^3 \alpha_{em}}{4 G_F^2} |\mathcal{A}|^2 \text{BR}(\mu \rightarrow e \bar{\nu}_e \nu_\mu), \quad (4.1)$$

where α_{em} is the fine-structure constant, G_F is the Fermi constant, and $\text{BR}(\mu \rightarrow e \bar{\nu}_e \nu_\mu)$ is approximately equal to unity. The dipole amplitude entering Eqn. (4.1) is

$$\mathcal{A} = \frac{Y_{11}^* Y_{21}}{32\pi^2 m_{\eta^+}^2} \mathcal{G}(y), \quad (4.2)$$

where m_{η^+} is the mass of the charged scalar field η^+ , and Y_{11} and Y_{21} are the corresponding elements of the rotated Yukawa coupling matrix in the charged-lepton mass basis. This rotated Yukawa matrix is defined as $Y = \beta_L U_L^\dagger (Y_1^4, Y_3^4, Y_2^4)^T$, where U_L is the unitary matrix that diagonalizes the charged-lepton mass matrix. Throughout our numerical analysis we fix $m_{\eta^+} = m_{\eta_I}$. The loop argument is defined as $y = \frac{M_f^2}{m_{\eta^+}^2}$, where M_f is the mass of the fermion propagating in the loop.

The loop function $\mathcal{G}(y)$ appearing in Eqn. (4.2) is

$$\mathcal{G}(y) = \frac{1 - 6y + 3y^2 + 2y^3 - 6y^2 \ln y}{6(1 - y)^4}. \quad (4.3)$$

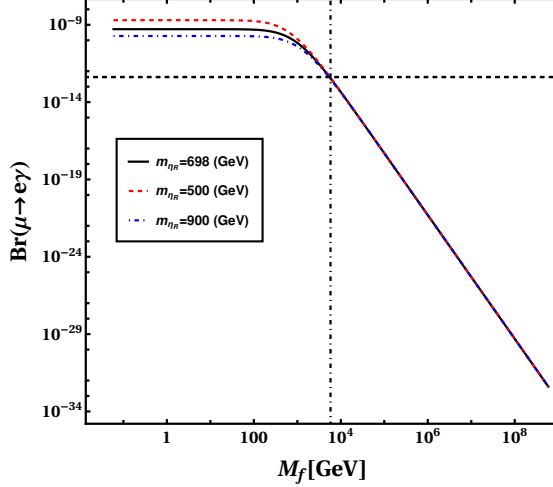


Figure 4: The correlation between mass of dark-sector fermion (f) and LFV branching ratio $\text{Br}(\mu \rightarrow e\gamma)$ for three different values of scalar mass $m_{\eta_R} \sim m_{\eta_1}$, while keeping all other parameters fixed at their best-fit values given in Table 5. The horizontal dashed line shows the current experimental upper bound on $\text{Br}(\mu \rightarrow e\gamma)$. The vertical dot-dashed line indicates the lower bound on the fermion mass M_f required to satisfy the LFV constraint.

The value of branching ratio predicted at the best-fit point, corresponding to the minimum of the χ^2 , is presented in Table 5. To illustrate how $\text{Br}(\mu \rightarrow e\gamma)$ varies with the mass of the fermion f and the real scalar mass m_{η_R} circulating in the loop, we fix all other parameters at their best-fit values and compute the resulting correlation for three representative values of m_{η_R} . The black curve corresponds to the best-fit point, while the other two curves represent the maximum and minimum values of m_{η_R} obtained from our data, as shown in Fig. 4. As seen in the figure, for relatively low fermion masses, up to about 10^3 GeV, the suppression is weak and $\text{Br}(\mu \rightarrow e\gamma)$ remains nearly constant and above the current experimental limit. The loop contribution becomes increasingly suppressed, and the branching ratio falls below the experimental upper bound for $M_f \gtrsim 6 \times 10^3$ GeV, irrespective of the mass m_{η_R} .

5 Leptogenesis

In Type-I seesaw framework, successful thermal leptogenesis typically requires a high scale $\mathcal{O}(10^9)$ GeV, known as the Davidson–Ibarra bound, to simultaneously account for neutrino masses and the observed baryon asymmetry. To evade this bound and realize leptogenesis at a lower scale, additional CP-violating contributions beyond the minimal seesaw setting are necessary. These contributions are often originates *via* new interactions or loop-induced effects involving extra states in non-holomorphic realization of scoto-seesaw modular framework. To this end, we consider the participation of dark sector particles in the leptogenesis dynamics, assuming a BSM fermion mass hierarchy $M_{N_1} < M_f \ll M_{N_2}$, for which the inverse decays and scatterings involving N_2 are Boltzmann suppressed. Consequently, at temperatures $T \sim M_{N_2}$, the interactions of the heavier fermion N_2 remain in thermal equilibrium, leading to an efficient washout of any lepton asymmetry it may gen-

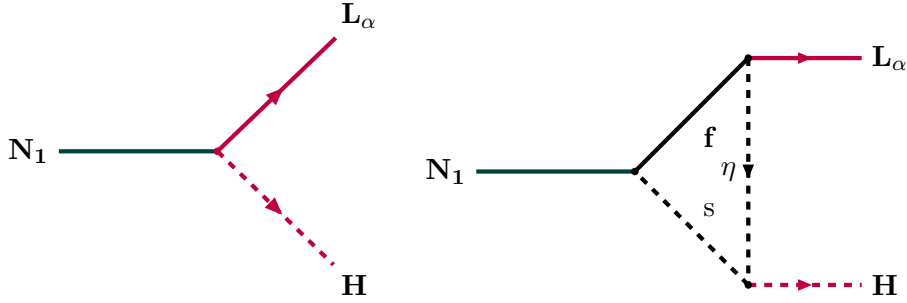


Figure 5: The tree and one-loop levels Feynman diagrams for dark-sector portal leptogenesis.

Benchmark Point	M_{N_1} (GeV)	M_η (GeV)	Δm^2 (GeV)	μ_s (GeV)	μ_1 (GeV)	M_f (GeV)	$\text{Re}[\tau]$	$\text{Im}[\tau]$
BP1	1.21×10^6	6.98×10^2	9.87×10^{-3}	10^3	10^4	3.09×10^7	0.26	0.98
BP2	1.28×10^6	6.02×10^2	9.97×10^{-3}	10^3	5×10^3	3.40×10^7	0.25	0.98
BP3	1.23×10^6	6.23×10^2	9.96×10^{-3}	10^3	10^3	3.24×10^7	0.25	0.98

Table 6: The best-fit values for the neutrino oscillation parameters obtained from the χ^2 analysis correspond to a minimum χ^2 value of 0.28 for NH.

erate. Consequently, successful leptogenesis proceeds solely through the out-of-equilibrium decay of N_1 . For simplicity, we work in the single-flavor approximation, which captures the qualitative behavior of the asymmetry. It is worth noting that the model, also, contains a viable candidate for dark matter. In particular, the CP-even neutral scalar originating from the inert doublet, η_1 , can play the role of dark matter provided it is the lightest among κ -odd particle. To ensure that the dark matter is predominantly the doublet component (rather than the singlet s), the mixing between the two CP-even states must remain small. This requirement, in Eqn. (2.8), translates into the conditions

$$A < B, \quad |C| \ll |A - B|, \quad (5.1)$$

where

$$A = \mu_\eta^2 + \frac{1}{2}(\lambda_3 + \lambda_4 - \lambda_5)v^2, \quad B = \mu_s^2 \quad (\text{for } \lambda_8 \rightarrow 0), \quad C = \mu_1 v. \quad (5.2)$$

Under these conditions, the lighter mass eigenstate is dominantly composed of η_1 and thus serves as the dark matter candidate.

The CP asymmetry,

$$\epsilon_1 = \frac{\Gamma(N_1 \rightarrow LH) - \Gamma(N_1 \rightarrow \bar{L}H^\dagger)}{\Gamma(N_1 \rightarrow LH) + \Gamma(N_1 \rightarrow \bar{L}H^\dagger)} = \frac{\Gamma(N_1 \rightarrow LH) - \Gamma(N_1 \rightarrow \bar{L}H^\dagger)}{\Gamma_N}, \quad (5.3)$$

generated in the decay of N_1 , shown in Fig. 5, arises from the interference between the tree-level and one-loop diagrams which, further, can be written as [83, 84]

$$\epsilon_1 = \frac{1}{8\pi} \frac{\text{Im}[\mathcal{M}_{\text{tree}}^* \mathcal{M}_{\text{loop}}]}{|\mathcal{M}_{\text{tree}}|^2}, \quad (5.4)$$

$$\epsilon_1 = \frac{1}{8\pi} \frac{\text{Im}(y_D^\dagger y_f y_1 \mu_1)}{(y_D^\dagger y_D) M_{N_1} (1 - \vartheta + \omega) \sqrt{(1 - \vartheta + \omega)^2 - 4\omega}} I_{\text{loop}}, \quad (5.5)$$

where

$$I_{\text{loop}} = 1 + \vartheta - 2\sqrt{\varsigma} + (\varsigma - \sqrt{\varsigma}(1 - \vartheta + \omega) - \varrho + \omega) \ln \left[\frac{\varsigma - (1 - \sqrt{\varsigma})^2}{\varsigma - \varsigma + \vartheta} \right],$$

is the loop function arises from vertex corrections involving the dark-sector fermion f , inert scalars and $y_D = U_L^\dagger M_D/v$. The mass ratios are defined as,

$$\varsigma = \frac{M_f^2}{M_{N_1}^2}, \quad \varrho = \frac{m_h^2}{M_{N_1}^2}, \quad \vartheta = \frac{m_h^2}{M_{N_1}^2}, \quad \omega = \frac{m_l^2}{M_{N_1}^2}, \quad \varsigma = \frac{m_s^2}{M_{N_1}^2}. \quad (5.6)$$

All CP-violating phases entering ϵ_1 originate from the complex modular forms. With the modular symmetry constraints, the Yukawa couplings in our model are determined by modular forms

$$y_f = \beta_L Y_3^{(4)}, \quad y_1 = a Y_3^{(2)}. \quad (5.7)$$

In the limit of vanishing SM Higgs and lepton masses, the CP asymmetry simplifies to

$$\epsilon_1 = \frac{1}{8\pi} \frac{\text{Im}(y_D^\dagger y_f y_1 \mu_1)}{(y_D^\dagger y_D) M_{N_1}} \left(1 - 2\sqrt{\varsigma} + (\varsigma - \sqrt{\varsigma} - \varrho) \ln \left[\frac{\varsigma - (1 - \sqrt{\varsigma})^2}{\varsigma - \varsigma} \right] \right). \quad (5.8)$$

The corresponding Boltzmann equations for co-moving densities of N_1 and $B - L$ can be written as

$$\begin{aligned} \frac{dY_{N_1}}{dz} = & -D_N \left(Y_{N_1} - Y_{N_1}^{\text{eq}} \right) - \frac{s}{H(z)z} \left(Y_{N_1}^2 - \left(Y_{N_1}^{\text{eq}} \right)^2 \right) \left[\langle \sigma v \rangle_{N_1 N_1 \rightarrow ss} + \langle \sigma v \rangle_{N_1 N_1 \rightarrow HH^\dagger} \right. \\ & \left. + \langle \sigma v \rangle_{N_1 N_1 \rightarrow L_\alpha \bar{L}_\beta} \right] - \frac{s}{H(z)z} \left(Y_{N_1} - Y_{N_1}^{\text{eq}} \right) \left[2Y_l^{\text{eq}} \langle \sigma v \rangle_{\bar{l} N_1 \rightarrow \bar{q} t} + 4Y_t^{\text{eq}} \langle \sigma v \rangle_{N_1 t \rightarrow \bar{l} q} \right. \\ & \left. + 2Y_s^{\text{eq}} \langle \sigma v \rangle_{N_1 s \rightarrow \bar{L} \eta^\dagger} + 2Y_H^{\text{eq}} \langle \sigma v \rangle_{N_1 H \rightarrow l_\alpha V_\mu} + 2y_f^{\text{eq}} \langle \sigma v \rangle_{N_1 f \rightarrow H \eta^\dagger} \right], \end{aligned} \quad (5.9)$$

$$\begin{aligned} \frac{dY_{B-L}}{dz} = & -\epsilon_1 D_N \left(Y_{N_1} - Y_{N_1}^{\text{eq}} \right) - W_{\text{ID}} Y_{B-L} - \frac{s}{H(z)z} Y_{B-L} \left[2Y_H^{\text{eq}} \langle \sigma v \rangle_{l H^\dagger \rightarrow \bar{L} H} + Y_{N_1} \langle \sigma v \rangle_{\bar{L} N_1 \rightarrow \bar{q} t} \right. \\ & \left. + 2Y_q^{\text{eq}} \langle \sigma v \rangle_{\bar{L} q \rightarrow N_1 t} + 2Y_l^{\text{eq}} \langle \sigma v \rangle_{L L \rightarrow H^\dagger H^\dagger} + Y_\eta^{\text{eq}} \langle \sigma v \rangle_{\bar{L} \eta^\dagger \rightarrow N_1 s} + Y_V^{\text{eq}} \langle \sigma v \rangle_{\bar{L} V_\mu \rightarrow H N_1} \right]. \end{aligned} \quad (5.10)$$

Here $Y_i = n_i/s$ denotes comoving density with n_i being number density of species ‘ i ’ and $\rho_s = \frac{2\pi^2}{45} g_* T^3$ being entropy density of the Universe. $z = M_{N_1}/T$ and $H(z) = \sqrt{\frac{4\pi^3 g_*}{45}} \frac{T^2}{M_{\text{Pl}}}$ is the Hubble parameter at high temperatures. The decay term D_N is defined as

$$D_N = \frac{\langle \Gamma_N \rangle}{H z} = K_N z \frac{\kappa_1(z)}{\kappa_2(z)}, \quad (5.11)$$

where $K_N = \Gamma_N/H(z=1)$ with $\kappa_i(z)$ being the modified Bessel function of i^{th} kind. The washout due to inverse decay (ID) is

$$W_{\text{ID}} = \frac{1}{4} K_N z^3 \kappa_1(z). \quad (5.12)$$

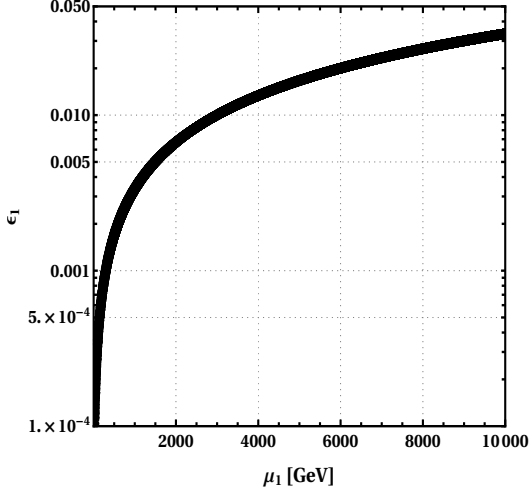


Figure 6: The correlation between CP asymmetry (ϵ_1) as function of dimensionful coupling μ_1 keeping other parameters fixed using Table 4.

The thermal averaged cross-section is defined as

$$\langle \sigma v \rangle_{ij \rightarrow kl} = \frac{1}{8T m_i^2 m_j^2 \kappa_2(z_i) \kappa_2(z_j)} \int_{(m_i+m_j)^2}^{\infty} ds \frac{\lambda(\rho_s, m_i^2, m_j^2)}{\sqrt{\rho_s}} \kappa_1(\sqrt{\rho_s}/T) \sigma, \quad (5.13)$$

with $z_i = m_i/T$ and $\lambda(\rho_s, m_i^2, m_j^2) = [\rho_s - (m_i + m_j)^2][\rho_s - (m_i - m_j)^2]$. The lepton asymmetry at the sphaleron decoupling epoch $T_{\text{sph}} \sim 130$ GeV gets converted into baryon asymmetry as

$$Y_B \simeq a_{\text{Sph}} Y_{B-L} = \frac{8 N_F + 4 N_H}{22 N_F + 13 N_H} Y_{B-L} = 0.34 Y_{B-L}, \quad (5.14)$$

with $N_F = 3, N_H = 2$ being the fermion generations and the number of scalar doublets in our model, respectively.

The dependence of the CP asymmetry parameter ϵ_1 on the trilinear coupling μ_1 is shown in Fig. 6 where all other parameters are fixed according to Table 4. We observe that increasing μ_1 leads to a substantial enhancement of the asymmetry parameter ϵ_1 as $\epsilon_1 \propto \mu_1$ Eqn. (5.8). Though increasing μ_1 enhances the CP asymmetry, for sufficiently large values of μ_1 (e.g. $\mu_1 \sim 10^4$ GeV) the resulting ϵ_1 can become as large as $\mathcal{O}(1)$, which in turn leads to a $B-L$ asymmetry exceeding the value required to reproduce the observed baryon asymmetry. This indicates that μ_1 cannot be arbitrarily increased, and successful leptogenesis imposes an upper bound on the trilinear coupling μ_1 to prevent the overproduction of the baryon asymmetry. The numerical results for the comoving number density of N_1 (left panel) and the $B - L$ asymmetry (right panel) are presented in Fig. 7. With the evolution of the Universe or increase in z , the N_1 starts decaying to the SM particles (Fig. 5), therefore reducing their respective comoving number densities. Fig. 7 (left panel) shows the evolution of the comoving number density of N_1 as a function of $z = M_{N_1}/T$ for the three benchmark points considered. At early times ($z \ll 1$), all solutions closely track the equilibrium distribution $Y_{N_1}^{\text{eq}}$, as expected for a relativistic species efficiently coupled to the

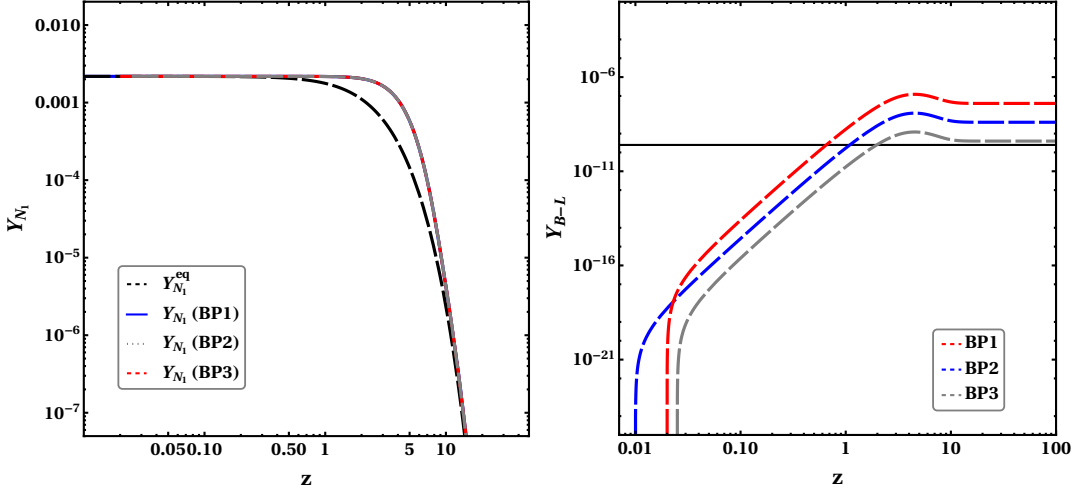


Figure 7: **Left panel:** The evolution of comoving number density of N_1 for different benchmark points given in Table 6. **Right panel:** The evolution of comoving number density of $B - L$ asymmetry for different benchmark points. The solid horizontal line corresponds to the experimentally required value of the lepton asymmetry (using Eqn. 5.14).

thermal bath. As the temperature drops below M_{N_1} , the equilibrium abundance decreases, while the actual abundance departs from equilibrium and begins to freeze out.

For all benchmark points, the number density Y_{N_1} remains slightly above the equilibrium value during the freeze-out phase. This mild departure from equilibrium reflects the fact that the decay and scattering interactions of N_1 are still moderately efficient around $z \sim \mathcal{O}(1-10)$, delaying the freeze-out relative to the purely equilibrium expectation. The three benchmark curves overlap throughout the evolution, indicating that the corresponding variations in the Yukawa couplings or dark-sector parameters have only a sub-leading impact on the dynamics of N_1 depletion. As a consequence, the CP-asymmetry-producing decays take place in a regime where N_1 is slightly over-abundant compared to equilibrium, ensuring a non-zero departure from equilibrium.

The evolution of $B - L$ asymmetry for three benchmark points (Table 6) is shown in right panel of Fig. 7. In all cases, the asymmetry begins to build up once the decays of N_1 start to dominate over inverse decay and scattering washout processes. Since the Dirac Yukawa coupling is fixed to a small value $y_D \sim 10^{-6}$ by neutrino oscillation data, the inverse-decay washout term, which scales as $\Gamma_{\text{ID}} \propto y_D^2$, remains weak throughout the relevant temperature range. Consequently, the washout rate Γ_{ID}/H becomes inefficient at relatively early times, allowing the generated CP asymmetry to accumulate smoothly.

A distinctive feature of this framework is that the dark-sector responsible for CP violation is controlled by the trilinear parameter μ_1 while the effective washout involving dark-sector fields depends on the fixed parameter $\mu_s = 1$ TeV. For simplicity, μ_s is kept the same for all benchmark points, such that the s -mediated washout channels remain moderately suppressed. Moreover, the kinematic hierarchy $M_{N_1} \sim 10^6$ GeV $< M_f \sim 10^7$ GeV for-

bids on-shell $N_1 N_1 \rightarrow f f$ scatterings thereby eliminating an otherwise potentially strong source of thermal washout. The remaining scattering channels, such as $N_1 N_1 \rightarrow H H^\dagger$ and $N_1 N_1 \rightarrow L \bar{L}$, are further suppressed due to their dependence on the small Yukawa coupling y_D and the relatively small inert-scalar mass splitting Δm^2 .

The benchmark points in Table 6 correspond to progressively smaller values of μ_1 , leading to different magnitudes of the loop-induced CP asymmetry. As a result, BP1 produces the largest final asymmetry, followed by BP2 and BP3, as reflected in Fig. 7 (right panel). In all benchmarks, the $B-L$ asymmetry saturates around $z \sim 10$ corresponding to the epoch at which N_1 fully departs from equilibrium and washout effects become negligible. The resulting asymmetries are compatible with the value required to reproduce the observed baryon asymmetry of the Universe after sphaleron conversion, demonstrating that the model can successfully realize leptogenesis without invoking resonant enhancement. The lightest dark sector particle, *i.e.* real part of inert scalar, is our viable dark matter particle (WIMP type) in the model which has been widely explored in the literature [84, 85]. A distinctive prediction of our construction arises from the inert scalar sector, in which the charged scalar η^\pm is nearly degenerate with the dark matter candidate η_1 . For the benchmark point, with $\delta m = m_{\eta^\pm} - m_{\eta_1} \sim 0.1$ GeV, the decay $\eta^\pm \rightarrow \eta_1 + W^{\pm*}$ proceeds only through an off-shell W boson and is therefore phase-space suppressed. Since $m_{\eta^\pm} - m_{\eta_R} \ll m_W$, the resulting decay width scales as $\Gamma \propto (\delta m)^5$ leading to a macroscopic decay length of $c\tau_{\eta^\pm} \sim \mathcal{O}(1-10)$ cm. Consequently, η^\pm behaves as a long-lived charged particle inside ATLAS/CMS experiments. The ATLAS Collaboration has recently performed a dedicated search for long-lived charged states using the full 140 fb^{-1} dataset of pp collisions at $\sqrt{s} = 13$ TeV. The analysis exploits signatures characterized by high specific ionization energy loss and time-of-flight measurements [86]. Interpreting their results³ in the context of stau-to-gravitino decays, ATLAS excludes masses up to 560 GeV for such long-lived charged particles. Observation of such a long-lived charged particle signal would provide strong support for the inert scalar sector of the model and offer an important experimental handle on the dark-sector-assisted origin of neutrino masses and leptogenesis.

6 Conclusion

This work investigates the neutrino phenomenology and dark-sector assisted leptogenesis in a scoto-seesaw framework constructed under a non-holomorphic A_4 modular flavor symmetry. To ensure a clean separation between the fields responsible for the tree-level (seesaw) and loop-induced (scotogenic) contributions to the neutrino mass matrix, we assign even modular weights to the fields in the seesaw sector and odd modular weights to those in the radiative sector. This modular-weight arrangement forbids undesired mixing terms and enforces a controlled hierarchical structure between these two neutrino mass-generating sectors. By restricting the complex modulus τ to lie within its fundamental domain and performing a systematic numerical scan over the remaining model parameters, we identify regions of parameter space that are fully consistent with the latest neutrino global-fit data. We find that the data is satisfied for $\text{Re}[\tau] \sim \pm 0.26$ and $\text{Im}[\tau] \sim 0.97$. Also, the

³The same interpretation has been inferred in Ref. [87].

CP violating phase δ is lying $\sim 70^\circ$ and $\sim 290^\circ$. The model is consistent only with a normal hierarchical neutrino mass pattern. In this setup, the complex modulus τ acts as the unique source of CP violation, since all Yukawa couplings and scalar-sector parameters are taken to be real. Consequently, the predicted low-energy neutrino mixing phases and the high-energy CP-violating interactions, relevant for leptogenesis, are entirely determined by the modular origin of flavor sector. Within this construction, successful leptogenesis emerges from the CP-violating out-of-equilibrium decays of the lightest right-handed neutrino N_1 into SM leptons and the Higgs doublet at $M_{N_1} \sim 10^6$ GeV. The loop-induced CP asymmetry is generated through one-loop diagrams mediated by the dark-sector fields intrinsic to the scotogenic mechanism, notably, without relying on any mass degeneracy or resonance enhancement between the heavy neutrino states. This demonstrates that the interplay of modular flavor structures and radiative dynamics can, naturally, accommodate the observed baryon asymmetry of the Universe while simultaneously reproducing the correct neutrino mass and mixing pattern. Finally, we have, also, incorporated a comment on the unique collider signature of η^\pm which may behave as a long-lived charged particle at ATLAS/CMS experiments.

Acknowledgments

The work of SN is supported by the United Arab Emirates University (UAEU) under UPAR Grant No. 12S162. LS acknowledges the financial support provided by the Council of Scientific and Industrial Research (CSIR) vide letter No. 09/1196(18553)/2024-EMR-I. Tapender acknowledges the financial support provided by Central University of Himachal Pradesh in the form of freeship. The authors, also, acknowledge Department of Physics and Astronomical Science for providing necessary facility to carry out this work.

A Non-Holomorphic Modular Flavor Symmetry

The conventional modular flavor symmetry employs holomorphic modular forms as Yukawa couplings, a structure naturally emerging in supersymmetric settings. However, modular invariance alone does not necessitate holomorphicity. By relaxing this condition, we enter the broader framework of *non-holomorphic modular symmetry*, where Yukawa couplings are polyharmonic Maass forms - automorphic functions satisfying the harmonic condition

$$\Delta_k Y(\tau) = 0, \quad (\text{A.1})$$

with $\Delta_k = -4y^2\partial_\tau\partial_{\bar{\tau}} + 2iky\partial_{\bar{\tau}}$ being the weight- k hyperbolic Laplacian, rather than requiring holomorphicity. These functions transform covariantly under the modular group:

$$Y(\gamma\tau) = (c\tau + d)^k \rho(\gamma) Y(\tau), \quad \gamma \in \text{SL}(2, \mathbb{Z}), \quad (\text{A.2})$$

where ρ denotes a representation of the finite modular group $\Gamma'_N = \text{SL}(2, \mathbb{Z})/\Gamma(N)$ (or Γ_N for even weight). Their Fourier expansion reveals the characteristic non-holomorphic

structure:

$$Y(\tau) = \sum_{n \geq 0} c^+(n)q^n + c^-(0)y^{1-k} + \sum_{n < 0} c^-(n)\Gamma(1-k, -4\pi ny)q^n, \quad (\text{A.3})$$

where the terms proportional to $c^-(0)$ and $c^-(n)$ explicitly break holomorphicity.

A crucial connection to ordinary modular forms exists via differential operators: the Maass raising operator D^{1-k} and the ξ -operator $\xi_k = 2iy^k\overline{\partial_\tau}$ map weight- k polyharmonic Maass forms to weight- $(2-k)$ modular forms in conjugate and original representations, respectively. This enables explicit construction of polyharmonic forms from known modular forms through the relations

$$\xi_k Y_{\mathbf{r}}^{(k)}(\tau) = \alpha \Omega Y_{\mathbf{r}'}^{(2-k)}(\tau), \quad (\text{A.4})$$

$$D^{1-k} Y_{\mathbf{r}}^{(k)}(\tau) = \beta Y_{\mathbf{r}}^{(2-k)}(\tau), \quad (\text{A.5})$$

where Ω relates conjugate representations and α, β are normalization constants.

In flavor model building, matter fields ψ_i are assigned modular weights $-k_i$ and transform in irreducible representations ρ_i of Γ'_N . Yukawa couplings are now polyharmonic Maass forms $Y_{\mathbf{r}}^{(k_Y)}(\tau)$ of weight k_Y and representation \mathbf{r} . Modular invariance imposes the conditions

$$k_Y = k_{\psi^c} + k_\psi + k_H, \quad (\text{A.6})$$

$$\rho_Y \otimes \rho_{\psi^c} \otimes \rho_\psi \otimes \rho_H \ni \mathbf{1}. \quad (\text{A.7})$$

This non-holomorphic extension significantly expands the Yukawa coupling space while preserving modular invariance. Negative modular weights become admissible, and non-holomorphic terms introduce new parameters that enhance phenomenological flexibility. The vacuum expectation value of τ simultaneously breaks modular and CP symmetries, offering a unified origin for flavor structures and CP violation. As an illustrative example, at level $N = 3$ (finite group A_4), polyharmonic Maass forms exist for weights $k = -4, -2, 0, 2, 4, 6, \dots$, organizing into A_4 multiplets, thereby enabling novel texture constructions beyond the holomorphic paradigm.

References

- [1] SUPER-KAMIOKANDE collaboration, *Evidence for oscillation of atmospheric neutrinos*, *Phys. Rev. Lett.* **81** (1998) 1562 [[hep-ex/9807003](#)].
- [2] SNO collaboration, *Direct evidence for neutrino flavor transformation from neutral current interactions in the Sudbury Neutrino Observatory*, *Phys. Rev. Lett.* **89** (2002) 011301 [[nucl-ex/0204008](#)].
- [3] DAYA BAY collaboration, *Observation of electron-antineutrino disappearance at Daya Bay*, *Phys. Rev. Lett.* **108** (2012) 171803 [[1203.1669](#)].
- [4] DOUBLE CHOOZ collaboration, *Indication for the disappearance of reactor electron antineutrinos in the Double Chooz experiment*, *Phys. Rev. Lett.* **108** (2012) 131801 [[1112.6353](#)].

[5] KamLAND collaboration, *First results from KamLAND: Evidence for reactor anti-neutrino disappearance*, *Phys. Rev. Lett.* **90** (2003) 021802 [[hep-ex/0212021](#)].

[6] SNO collaboration, *Measurement of the rate of $\nu_e + d \rightarrow p + p + e^-$ interactions produced by 8B solar neutrinos at the Sudbury Neutrino Observatory*, *Phys. Rev. Lett.* **87** (2001) 071301 [[nucl-ex/0106015](#)].

[7] S. Weinberg, *Baryon and Lepton Nonconserving Processes*, *Phys. Rev. Lett.* **43** (1979) 1566.

[8] Y. Cai, J. Herrero-García, M.A. Schmidt, A. Vicente and R.R. Volkas, *From the trees to the forest: a review of radiative neutrino mass models*, *Front. in Phys.* **5** (2017) 63 [[1706.08524](#)].

[9] P.-H. Gu, *Weinberg dimension-5 operator by vector-like lepton doublets*, [2006.08616](#).

[10] F. Bonnet, M. Hirsch, T. Ota and W. Winter, *Systematic study of the $d=5$ Weinberg operator at one-loop order*, *JHEP* **07** (2012) 153 [[1204.5862](#)].

[11] Y. Liao, *Unique Neutrino Mass Operator at any Mass Dimension*, *Phys. Lett. B* **694** (2011) 346 [[1009.1692](#)].

[12] M. Chala and A. Titov, *Neutrino masses in the Standard Model effective field theory*, *Phys. Rev. D* **104** (2021) 035002 [[2104.08248](#)].

[13] X. Li and S. Zhou, *One-loop matching of the type-III seesaw model onto the Standard Model Effective Field Theory*, *JHEP* **05** (2024) 169 [[2309.14702](#)].

[14] Y. Du, X.-X. Li and J.-H. Yu, *Neutrino seesaw models at one-loop matching: discrimination by effective operators*, *JHEP* **09** (2022) 207 [[2201.04646](#)].

[15] E. Ma, *Verifiable radiative seesaw mechanism of neutrino mass and dark matter*, *Phys. Rev. D* **73** (2006) 077301 [[hep-ph/0601225](#)].

[16] Tapender, L. Singh and S. Verma, *Dark matter and collider phenomenology in radiative Type-III seesaw model with two inert doublets*, *Phys. Dark Univ.* **50** (2025) 102085 [[2503.18566](#)].

[17] Tapender, S. Verma and S. Kumar, *On lepton flavor violation and dark matter in Scotogenic model with trimaximal mixing*, *Eur. Phys. J. Plus* **140** (2025) 43 [[2402.16491](#)].

[18] Tapender, S. Kumar and S. Verma, *Neutrino phenomenology in a model with generalized CP symmetry within type-I seesaw framework*, *Phys. Rev. D* **109** (2024) 015004 [[2309.04242](#)].

[19] L. Singh, Tapender, M. Kashav and S. Verma, *Trimaximal mixing and extended magic symmetry in a model of neutrino mass matrix*, *EPL* **142** (2023) 64002 [[2207.13328](#)].

[20] M. Kashav and S. Verma, *Broken scaling neutrino mass matrix and leptogenesis based on A_4 modular invariance*, *JHEP* **09** (2021) 100 [[2103.07207](#)].

[21] Priya, L. Singh, B.C. Chauhan and S. Verma, *Type-III Seesaw in Non-Holomorphic Modular Symmetry and Leptogenesis*, [2508.05047](#).

[22] L. Singh, M. Kashav and S. Verma, *Minimal type-I Dirac seesaw and leptogenesis under A_4 modular invariance*, *Nucl. Phys. B* **1007** (2024) 116666 [[2405.07165](#)].

[23] L. Singh, D. Mahanta and S. Verma, *Low scale leptogenesis in singlet-triplet scotogenic model*, *JCAP* **02** (2024) 041 [[2309.12755](#)].

[24] L. Singh, R. Srivastava, S. Verma and S. Yadav, *Type-III scotogenic model: Inflation, dark matter, and collider phenomenology*, *Phys. Rev. D* **112** (2025) 095014 [[2501.13171](#)].

[25] M. Kashav and S. Verma, *A₄ Flavor Model for Deviation in $\mu - \tau$ Reflection Symmetry with Type-I+II Seesaw Extensions*, *Int. J. Theor. Phys.* **62** (2023) 267.

[26] S. Verma, M. Kashav and S. Bhardwaj, *Highly predictive and testable A₄ flavor model within type-I and II seesaw framework and associated phenomenology*, *Nucl. Phys. B* **946** (2019) 114704 [[1811.06249](#)].

[27] J.N. Ng, *Neutrino mass models in extra dimensions*, *J. Korean Phys. Soc.* **45** (2004) S341 [[hep-ph/0311352](#)].

[28] N. Arkani-Hamed, S. Dimopoulos, G.R. Dvali and J. March-Russell, *Neutrino masses from large extra dimensions*, *Phys. Rev. D* **65** (2001) 024032 [[hep-ph/9811448](#)].

[29] M. Neubert, *Neutrino physics with small extra dimensions*, *Int. J. Mod. Phys. A* **16S1B** (2001) 704 [[hep-ph/0011063](#)].

[30] T. Asaka, Y. Heo, T.H. Tatsuishi and T. Yoshida, *Modular A₄ invariance and leptogenesis*, *JHEP* **01** (2020) 144 [[1909.06520](#)].

[31] G.-J. Ding, S.F. King, J.-N. Lu and B.-Y. Qu, *Leptogenesis in SO(10) models with A₄ modular symmetry*, *JHEP* **10** (2022) 071 [[2206.14675](#)].

[32] M.K. Behera and R. Mohanta, *Linear Seesaw in A5' Modular Symmetry With Leptogenesis*, *Front. in Phys.* **10** (2022) 854595 [[2201.10429](#)].

[33] G. Pathak and M.K. Das, *Matter-antimatter asymmetry in minimal inverse seesaw framework with A₄ modular symmetry*, [2505.03000](#).

[34] M. Kashav and S. Verma, *On minimal realization of topological Lorentz structures with one-loop seesaw extensions in A₄ modular symmetry*, *JCAP* **03** (2023) 010 [[2205.06545](#)].

[35] P. Mishra, M.K. Behera, P. Panda and R. Mohanta, *Type III seesaw under A₄ modular symmetry with leptogenesis*, *Eur. Phys. J. C* **82** (2022) 1115 [[2204.08338](#)].

[36] S. Marciano, D. Meloni and M. Parriciatu, *Minimal seesaw and leptogenesis with the smallest modular finite group*, *JHEP* **05** (2024) 020 [[2402.18547](#)].

[37] M.K. Behera, S. Mishra, S. Singirala and R. Mohanta, *Implications of A₄ modular symmetry on neutrino mass, mixing and leptogenesis with linear seesaw*, *Phys. Dark Univ.* **36** (2022) 101027 [[2007.00545](#)].

[38] R. Mohanta, M.K. Behera, S. Singirala and S. Mishra, *Implications of A₄ modular symmetry on neutrino mass, mixing and leptogenesis with linear seesaw*, *PoS FPCP2023* (2023) 063.

[39] Abhishek and V.S. Mummidi, *Resonant leptogenesis in inverse see-saw framework with modular S₄ symmetry*, [2507.06610](#).

[40] H.B. Nogueira, J.S.F. Neto, R.N.d.C. Filho and J.R.d.S. Leite, *Neutrino mass generation via the inverse seesaw mechanism in a U(1)_{B-L} gauge extension*, [2507.03795](#).

[41] S.K. Kang and C.S. Kim, *Extended double seesaw model for neutrino mass spectrum and low scale leptogenesis*, *Phys. Lett. B* **646** (2007) 248 [[hep-ph/0607072](#)].

[42] A.E. Cárcamo Hernández, Y.H. Velásquez, S. Kovalenko, N.A. Pérez-Julve and I. Schmidt, *Models of Radiative Linear Seesaw with Electrically Charged Mediators*, *PTEP* **2024** (2024) 103B02 [[2403.05637](#)].

[43] A.G. Dias, C.A. de S. Pires and P.S.R. da Silva, *How the Inverse See-Saw Mechanism Can Reveal Itself Natural, Canonical and Independent of the Right-Handed Neutrino Mass*, *Phys. Rev. D* **84** (2011) 053011 [[1107.0739](#)].

[44] E. Ma, *Inverse Seesaw Neutrino Mass from Lepton Triplets in the $U(1)(\text{Sigma})$ Model*, *Mod. Phys. Lett. A* **24** (2009) 2491 [[0905.2972](#)].

[45] A. Batra, P. Bharadwaj, S. Mandal, R. Srivastava and J.W.F. Valle, *Phenomenology of the simplest linear seesaw mechanism*, *JHEP* **07** (2023) 221 [[2305.00994](#)].

[46] A. Das, T. Nomura, H. Okada and S. Roy, *Generation of a radiative neutrino mass in the linear seesaw framework, charged lepton flavor violation, and dark matter*, *Phys. Rev. D* **96** (2017) 075001 [[1704.02078](#)].

[47] B.-Y. Qu and G.-J. Ding, *Non-holomorphic modular flavor symmetry*, *JHEP* **08** (2024) 136 [[2406.02527](#)].

[48] T. Nomura and H. Okada, *Type-II seesaw of a non-holomorphic modular A_4 symmetry*, *Phys. Lett. B* **868** (2025) 139763 [[2408.01143](#)].

[49] T. Nomura, H. Okada and O. Popov, *Non-holomorphic modular A_4 symmetric scotogenic model*, *Phys. Lett. B* **860** (2025) 139171 [[2409.12547](#)].

[50] T. Nomura and H. Okada, *Zee model in a non-holomorphic modular A_4 symmetry*, *Phys. Lett. B* **867** (2025) 139618 [[2412.18095](#)].

[51] T. Nomura, H. Okada and X.-Y. Wang, *A radiative neutrino mass model with leptoquarks under non-holomorphic modular A_4 symmetry*, *JHEP* **09** (2025) 163 [[2504.21404](#)].

[52] T. Nomura and H. Okada, *Neutrino mass model at a three-loop level from a non-holomorphic modular A_4 symmetry*, [2506.02639](#).

[53] T. Nomura and H. Okada, *A new type of lepton seesaw model in a modular A_4 symmetry*, [2503.19251](#).

[54] S.K. Kang and H. Okada, *Neutrino masses and mixing in an axion model*, *Eur. Phys. J. C* **85** (2025) 917 [[2408.14942](#)].

[55] G.-J. Ding, J.-N. Lu, S.T. Petcov and B.-Y. Qu, *Non-holomorphic modular S_4 lepton flavour models*, *JHEP* **01** (2025) 191 [[2408.15988](#)].

[56] C.-C. Li, J.-N. Lu and G.-J. Ding, *Non-holomorphic modular A_5 symmetry for lepton masses and mixing*, *JHEP* **12** (2024) 189 [[2410.24103](#)].

[57] H. Okada and Y. Orikasa, *A radiative seesaw in a non-holomorphic modular S_3 flavor symmetry*, [2501.15748](#).

[58] T. Kobayashi, H. Okada and Y. Orikasa, *Zee-Babu model in a non-holomorphic modular A_4 symmetry and modular stabilization*, [2502.12662](#).

[59] M.A. Loualidi, M. Miskaoui and S. Nasri, *Nonholomorphic A_4 modular invariance for fermion masses and mixing in $SU(5)$ GUT*, *Phys. Rev. D* **112** (2025) 015008 [[2503.12594](#)].

[60] X. Zhang and Y. Reyimuaji, *Inverse Seesaw Model in Non-holomorphic Modular A_4 Flavor Symmetry*, [2507.06945](#).

[61] T. Nomura and H. Okada, *Lepton seesaw model in a modular A_4 symmetry*, [2409.10912](#).

[62] M. Abbas, *Lepton Masses and Mixing in Nonholomorphic Modular A_4 Symmetry*, *PHEP* **2025** (2025) 7.

[63] C.-C. Li and G.-J. Ding, *Lepton models from non-holomorphic A'_5 modular flavor symmetry*, [2509.15183](#).

[64] M. Dey, *The Seesaw Evaded Modular Dirac Framework*, [2509.10373](#).

[65] S.K. Nanda, M. Ricky Devi and S. Patra, *Non-Holomorphic A_4 Modular Symmetry in Type-I Seesaw: Implications for Neutrino Masses and Leptogenesis*, [2509.22108](#).

[66] B. Kumar and M.K. Das, *Leptogenesis, $0\nu\beta\beta$ and lepton flavor violation in modular left-right asymmetric model with polyharmonic Maass forms*, *JHEP* **09** (2025) 071 [[2504.21701](#)].

[67] M. Fukugita and T. Yanagida, *Baryogenesis Without Grand Unification*, *Phys. Lett. B* **174** (1986) 45.

[68] S. Davidson, E. Nardi and Y. Nir, *Leptogenesis*, *Phys. Rept.* **466** (2008) 105 [[0802.2962](#)].

[69] W. Buchmuller, R.D. Peccei and T. Yanagida, *Leptogenesis as the origin of matter*, *Ann. Rev. Nucl. Part. Sci.* **55** (2005) 311 [[hep-ph/0502169](#)].

[70] C.S. Fong, E. Nardi and A. Riotto, *Leptogenesis in the Universe*, *Adv. High Energy Phys.* **2012** (2012) 158303 [[1301.3062](#)].

[71] A. Pilaftsis, *The Little Review on Leptogenesis*, *J. Phys. Conf. Ser.* **171** (2009) 012017 [[0904.1182](#)].

[72] J. Kubo and D. Suematsu, *Neutrino masses and CDM in a non-supersymmetric model*, *Phys. Lett. B* **643** (2006) 336 [[hep-ph/0610006](#)].

[73] N. Rojas, R. Srivastava and J.W.F. Valle, *Simplest Scoto-Seesaw Mechanism*, *Phys. Lett. B* **789** (2019) 132 [[1807.11447](#)].

[74] I. Esteban, M.C. Gonzalez-Garcia, M. Maltoni, I. Martinez-Soler, J.P. Pinheiro and T. Schwetz, *NuFit-6.0: updated global analysis of three-flavor neutrino oscillations*, *JHEP* **12** (2024) 216 [[2410.05380](#)].

[75] PARTICLE DATA GROUP collaboration, *Review of particle physics*, *Phys. Rev. D* **110** (2024) 030001.

[76] NOvA collaboration, *Improved measurement of neutrino oscillation parameters by the NOvA experiment*, *Phys. Rev. D* **106** (2022) 032004 [[2108.08219](#)].

[77] T2K collaboration, *Measurements of neutrino oscillation parameters from the T2K experiment using 3.6×10^{21} protons on target*, *Eur. Phys. J. C* **83** (2023) 782 [[2303.03222](#)].

[78] KamLAND-ZEN collaboration, *Search for Majorana Neutrinos with the Complete KamLAND-Zen Dataset*, [2406.11438](#).

[79] LEGEND collaboration, *First Results on the Search for Lepton Number Violating Neutrinoless Double Beta Decay with the LEGEND-200 Experiment*, [2505.10440](#).

[80] nEXO collaboration, *nEXO: neutrinoless double beta decay search beyond 10^{28} year half-life sensitivity*, *J. Phys. G* **49** (2022) 015104 [[2106.16243](#)].

[81] MEG collaboration, *Final Results of the MEG Experiment*, *Nuovo Cim. C* **39** (2017) 325 [[1606.08168](#)].

[82] T. Toma and A. Vicente, *Lepton Flavor Violation in the Scotogenic Model*, *JHEP* **01** (2014) 160 [[1312.2840](#)].

[83] D.M. Barreiros, H.B. Câmara, R.G. Felipe and F.R. Joaquim, *Scalar-singlet assisted leptogenesis with CP violation from the vacuum*, *JHEP* **01** (2023) 010 [[2211.00042](#)].

[84] D. Borah, D. Mahanta and I. Saha, *Gravitational wave signatures of dark sector portal leptogenesis*, [2504.14671](#).

- [85] S. Mandal, R. Srivastava and J.W.F. Valle, *The simplest scoto-seesaw model: WIMP dark matter phenomenology and Higgs vacuum stability*, *Phys. Lett. B* **819** (2021) 136458 [[2104.13401](#)].
- [86] ATLAS collaboration, *Search for long-lived charged particles using large specific ionisation loss and time of flight in 140 fb⁻¹ of pp collisions at $\sqrt{s} = 13$ TeV with the ATLAS detector*, *JHEP* **07** (2025) 140 [[2502.06694](#)].
- [87] S.-Y. Guo and M.-Y. Zhao, *Probing the Scotogenic Dirac Model with FIMP Dark Matter and ΔN_{eff}* , [2508.16362](#).